*Journal of Applied Fluid Mechanics*, Vol. 17, No. 3, pp. 591-603, 2024.
Available online at www.jafmonline.net, ISSN 1735-3572, EISSN 1735-3645.
https://doi.org/10.47176/jafm.17.3.2172

# Analysis of Cavitation-induced Vibration Characteristics of a Vortex Pump Based on Adaptive Optimal Kernel Time-frequency Representation

Y. Wang, P. Zhou†, C. Zhou, W. Zhou and J. Li

*College of Metrology & Measurement Engineering, China Jiliang University, Hangzhou, 310018, China*

†*Corresponding Author Email: zhoupj@cjlu.edu.cn*

## ABSTRACT

Cavitation-induced vibration presents a significant challenge in vortex pumps, leading to potential damage to hydraulic components and adverse effects on pump performance. This study aims to investigate the long-term implications of such phenomena. To capture the vibration signals caused by cavitation, we utilized vibration acceleration sensors on the vortex pump and collected data at five predetermined measuring points under three different operating conditions. The analysis used two prominent techniques, fast Fourier transform (FFT) and adaptive optimal kernel time-frequency representation (AOK-TFR), to explore the frequency-domain and time-frequency characteristics of the vibration signals. The findings reveal a notable increase in frequency amplitude at each monitoring point as the flow rate rises. Under cavitation conditions, pronounced vibration characteristics are observed along the y-axis and z-axis of the volute, with maximum vibration intensities of 1.83 m/s² and 1.80 m/s², respectively. The frequency amplitude exhibits non-constant behavior in the time series. Moreover, variations in the time-frequency characteristics are identified with changing flow rates. A distinct signal with a frequency of 750 Hz manifests in the x-axis and y-axis of the volute when the head experiences a 3% reduction from the cavitation level.

***Article History***

*Received July 18, 2023*
*Revised October 20, 2023*
*Accepted October 21, 2023*
*Available online January 1, 2024*

***Keywords:***

*Vortex pump*
*Cavitation characteristic*
*Vibration signal*
*Time-domain analysis*
*Frequency-domain analysis*
*Time-frequency distribution*

## 1. INTRODUCTION

The vortex pumps are widely applied in sewage treatment, water transportation, and industrial production due to their unique non-clogging characteristics (Wang et al., 2023). However, cavitation, a hydrodynamic phenomenon arising from the formation and violent collapse of vapor-filled cavities due to localized pressure drops, damages hydraulic machinery like centrifugal pumps and turbines, causing degradation in performance, erosion, and noise (Machalski et al., 2021; Mao et al., 2016; Song et al., 2014). It can also result in pipeline resonance, leading to severe vibrations and noise throughout the pump system (Hajnayeb, 2021; Dai, 2023).

Vortex pumps are susceptible to cavitation (Aoki, 1983), but there is a lack of research exploring the impacts of this phenomenon. Wu et al. (2016) conducted a cavitation performance test on two different models of vortex pumps and discovered that the net positive suction head available ($NPSH_a$) fluctuated within the specified range. Moreover, if the net positive suction head (*NPSH*) was low, the flow channel would be blocked by cavitation, resulting in a significant reduction in the head. Li (2017) showed that a vortex pump's cavitation performance was worse in turbine mode than in pump mode. The required net positive suction head ($NPSH_r$) of a turbine is 3.17 times more than that of a pump under optimal operating conditions. Steinmann et al. (2010) used high-speed photography to capture the instantaneous flow pattern in the vortex pump, and they found that the shape and size of the cavitation produced were constantly varying, with some of the cavitation collapsing near the impeller wall. Sha & Hou (2010) observed that the cavitation curve of the vortex pump was parabolic. They also discovered that once the optimal operating condition was reached, the *NPSH* increased with increasing flow rate. Although there has been significant research on cavitation performance, there is a lack of information on the vibration characteristics of vortex pumps in a cavitation state.

A fundamental approach to revealing cavitation in a pump is through vibration signal analysis, which provides

**NOMENCLATURE**

| | | | |
|---|---|---|---|
| $A$ | vibration amplitude | $NPSH_a$ | available net positive suction head |
| *AOK TFR* | Adaptive Optimal Kernel Time-Frequency Representation | $NPSH_r$ | required net positive suction head |
| $f_{BPF}$ | blade passing frequency | $n$ | rational speed |
| $f_{RF}$ | rotational frequency | $Q$ | pump flow rate |
| *FFT* | Fast Fourier Transform | *STFT* | Short-Time Fourier Transform |
| $H$ | pump head | *UIWG* | Unequal Interval Weight Grey |
| *NPSH* | Net Positive Suction Head | $Z_{rms}$ | the root-mean-square value of the vibration acceleration signal |

a detailed analysis of the cavitation-induced vibration characteristics in the pump. Based on the short-time Fourier transform (STFT) method, Li et al. (2018) found that the cavitation level can be judged by the narrow band frequency range of vibration signals in a centrifugal pump. Al-Obaidi (2019, 2020) studied how different operating conditions affect centrifugal pump cavitation by collecting the vibration signals of centrifugal pumps under cavitation at various flow rates and speeds and applying time-domain and frequency-domain analysis techniques. Lu et al. (2022) introduced a novel cavitation determination method, which relies on the dimensionless power ratio *r*. When *r*=2, cavitation is considered to occur in the pump. The accuracy and effectiveness of this method can be tested. Zhou et al. (2022) used vibration acceleration sensors and hydrophones to obtain cavitation-induced vibration signals of vortex pumps and compared the influence of monitoring points on cavitation. The cavitation volume distribution and pressure pulsation signals under different cavitation states are obtained by numerical simulation. Cao et al. (2021) used the unequal interval weight grey (UIWG) model to determine the relationship between vibration signals and *NPSH* and verified that the UIWG model has good robustness and high accuracy. The vibration signal of 2000Hz-5000Hz is considered to be stable and suitable for predicting the cavitation frequency range. Yao et al. (2011) analyzed the frequency-domain and time-frequency characteristics of pressure pulsation in a double-suction pump using the fast Fourier transform (FFT) and adaptive optimal kernel time-frequency representation (AOK-TFR). It was shown that the frequency-domain and time-frequency domain can clearly reflect that asymmetric pressure pulsation exists within the double-suction pump. Lu et al. (2017) discovered that vibration characteristics and cavitation state are intricately linked. The measurement point for vibration characteristics of cavitation should be positioned as close as possible to the flow channel and bubble source. A head reduction of 0.59% in the test pump indicates cavitation occurrence.

The present paper compares the cavitation experiments of a vortex pump under three conditions using the pump cavitation closed-loop test rig and analyses its vibration characteristics. The primary objective is to investigate the vibration signals of the pump under various monitoring flows in both the time and frequency domains using AOK-TFR. The study offers a significant addition to the vortex pump's vibration under a cavitation state and addresses the deficiencies in previous cavitation studies. Furthermore, it offers a vital reference for the cavitation diagnosis of vortex pumps.

## 2. ADAPTIVE OPTIMAL KERNEL TIME DISTRIBUTION

The AOK is a theory of time-frequency analysis based on an improved Wigner-Ville distribution. The window function is utilized to intercept a short-time fuzzy function denoted as $A(t,\theta,\tau)$ in the extracted signal.

$$A(t,\theta,\tau)=\int s^*(u-\frac{\tau}{2})\omega^*(u-t-\frac{\tau}{2})\bullet s(u+\frac{\tau}{2})\times\omega(u-t+\frac{\tau}{2})e^{j\theta u}du \quad (1)$$

Where $s(t)$ is the signal to be analyzed; $s^*(t)$is the conjugate function of $s(t)$; $\omega(u)$ is a symmetric window function; $t$ is the center position of $\omega(u)$. Let $\omega(u)=0$ for $|u|>T$. Then at any moment $t$, only the signal within $[t\text{-}T, t\text{+}T]$ can be calculated for its fuzzy function. For any detailed part of the signal, the short-time fuzzy function can be accurately portrayed. AOK TFR is defined as:

$$P_{AOK}(t,\omega)=\frac{1}{4\pi^2}\iint A(t,\theta,\tau)\phi_{opt}(t;\theta,\tau)e^{-j\theta t-j\tau\omega}d\theta d\tau \quad (2)$$

Where $\omega$ is the frequency variable; $(t;\theta,\tau)$ is the optimal kernel time function of the window function, which can be obtained by solving the optimization problem by Eq (3).

$$\max_{\phi}\int_0^{2\pi}\int_0^{\infty}|A(r,\psi)|\phi|r,\psi|^2\,rdrd\psi \quad (3)$$

The constraints are:

$$\phi(r,\psi)=\exp(-\frac{r^2}{2\sigma^2(\psi)}) \quad (4)$$

$$\frac{1}{4\pi^2}\int_0^{2\pi}\int_0^{\infty}|\phi(r,\psi)|^2\,rdrd\psi=\frac{1}{4\pi^2}\int_0^{2\pi}\sigma^2(\psi)d\psi\le\alpha,\alpha\ge 0 \quad (5)$$

Where $\phi(r,\psi)$ and $A(r,\psi)$ are the polar forms of the kernel functions $\phi(t;\theta,\tau)$ and $A(t,\theta,\tau)$, respectively; $r=\sqrt{\theta^2+\tau^2}$; $\psi=\arctan(\tau/\theta)$.

The AOK-TFR's kernel function dynamically adjusts based on the signal characteristics, efficiently suppressing distant mutual components in the fuzzy domain, while preserving the self-components concentrated near the origin. (Jones & Baraniuk, 1995). This method offers improved adaptability to changes in signal characteristics, thereby enhancing the accuracy of time-frequency analysis.

**Table 1 Hydraulic parameter of the vortex pump**

| Hydraulic parameter | Symbol | Numerical value |
|---|---|---|
| Rational speed | *n* | 2900 r/min |
| Pump flow rate | *Q* | 40 $m^3$/h |
| Pump head | *H* | 22 m |

**Table 2 Main geometric parameters of the test pump**

| Design Parameters | Numerical value |
|---|---|
| Inlet diameter | 70 mm |
| Outlet diameter | 70 mm |
| Blade width | 32 mm |
| Blade thickness | 4 mm |
| Number of blades | 10 |
| Impeller diameter | 134 mm |

Among the four time-frequency analysis methods compared, the AOK-TFR method demonstrates superior efficacy in mitigating noise and minimizing cross-term interference (Li et al. 2009). Therefore, the AOK-TFR is used as the time-frequency analysis method in this paper.

## 3. CAVITATION EXPERIMENTAL SETUP AND VIBRATION MEASUREMENT

### 3.1 Experimental Setup

The research focuses on a vortex pump, and Table 1 presents its corresponding hydraulic parameters. The occurrence of cavitation is determined by adopting a criterion of a 3% drop in the pump's head. The volute, impeller, inlet pipe, outlet pipe, and other flow components of the experimental pump are fabricated using Plexiglass, enabling visualization of the cavitation distribution within the pump via photography. In order to prevent the entry of external air into the pump through gaps during the cavitation experiment, we utilized silicone gaskets and neutral structural glue to effectively seal the connection between the inlet pipe and the volute. The parameters of the test pump can be observed in Table 2.

The experimental setup is mainly composed of three parts: a closed-loop test rig, high-speed camera and a vibration signal acquisition system, where the closed-loop test rig is shown in Fig. 1 and Fig. 2.

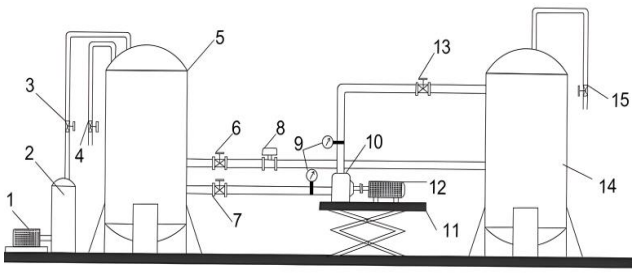


1-Vacuum pump, 2-Cavitation cylinder, 3-Valve, 4-Valve, 5-Cavitation tank, 6-Cavitation tank inlet valve, 7-Cavitation tank outlet valve, 8-Electromagnetic flow meter, 9-Import and export pressure gauge, 10-Test pump, 11-Lift table, 12-Motor, 13-Stabilizer tank inlet valve, 14-Stabilizer tank, 15-Valve.

**Fig. 1 Closed-loop test rig**

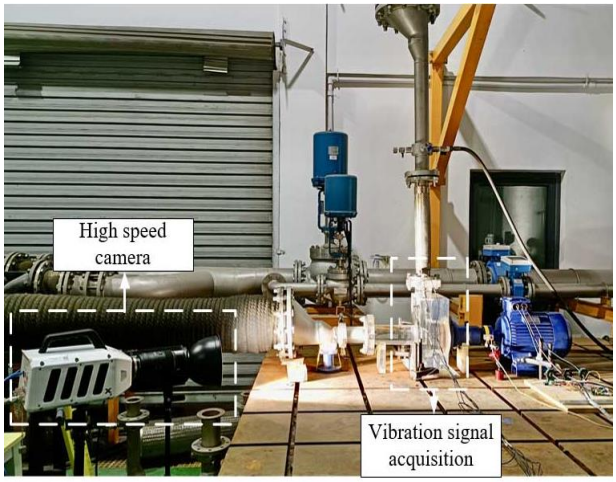


**Fig. 2 Experimental system site**

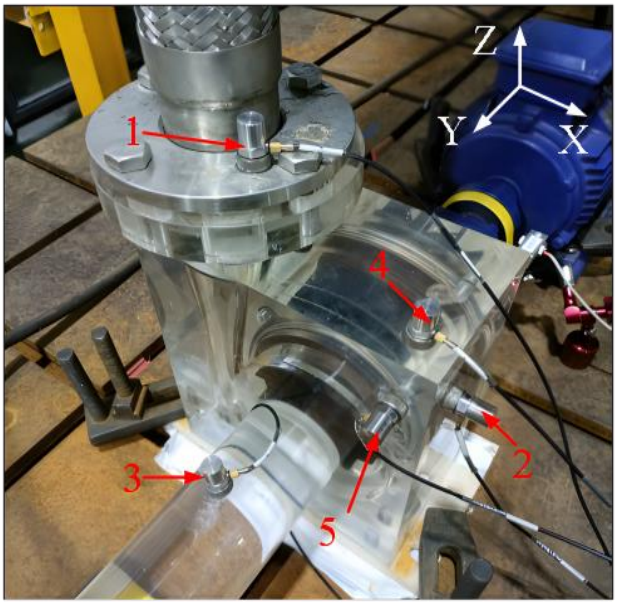


1 - Outlet pipe z-axis, 2 - Volute x-axis, 3 - Inlet pipe z-axis, 4-Volute z-axis, 5-Volute y-axis

**Fig. 3 Acceleration sensor mounting position**

### 3.2 Vibration Measurement

The vibration signal in this experiment is collected using the 1A111E vibration acceleration sensor, which has a frequency response ranging from 0.5 kHz to 7 kHz. As shown in Fig. 3, the radial direction is designated as the x-axis, the axial direction as the y-axis, and the exit direction of the volute as the z-axis. Five vibration measurement points were selected, and the vibration sensors were placed in the z-axis direction of the inlet and outlet pipes and the volute's x-axis, y-axis, and z-axis directions. To ensure the accuracy of the test, this test measured the vibration value of the vortex pump at a standstill and rated operating conditions; the vibration value at a standstill is about 0.02 times the vibration value at rated operating conditions. Therefore, this experiment is subject to less interference from external vibration and can be conducted. The sampling frequency of the sensor is set to 10000 Hz for this experiment. Figure 4 displays the flow chart of the cavitation experiment.

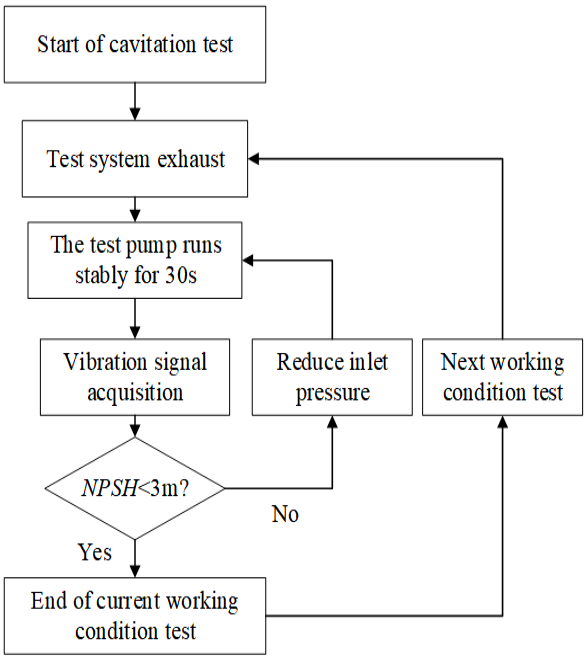


**Fig. 4 Cavitation test procedure**

## 4. RESULTS AND ANALYSIS

### 4.1 Cavitation Experiment Results

In three different operating conditions, the inlet and outlet pressures of the vortex pump were collected independently. The Net Positive Suction Head available (*NPSH*a) was computed using Eq (6), and the resulting cavitation performance curves for various flow rates were plotted, as depicted in Fig 5. As the *NPSH* decreases, there will be a gradual reduction in head until cavitation occurs, at which point the rate of head decrease becomes significantly more pronounced. The increase in flow rate reduces the inlet pressure of the vortex pump, causing the vortex pump's performance to deteriorate. When the head decreases by 3%, the *NPSH* is 2.77 m, 3.53 m, and 4.34 m for flow rates of 35 $m^3/h$, 40 $m^3/h$, and 45 $m^3/h$, respectively.

$$NPSH_a = \frac{P_C}{\rho g} - h_g - h_c - \frac{P_V}{\rho g} \tag{6}$$

Where $P_c$ is the absolute pressure of the suction surface; $h_g$ is the vertical distance from the pump to the liquid surface at the inlet; $h_c$ is the head loss of the inlet pipeline; $P_v$ is the vaporization pressure at transient temperature.

Figures 6, 7, and 8 illustrate the distribution of cavitation for the following scenarios: non-cavitation, visual incipient cavitation, cavitation states of 1% head drop ($\Delta H$=1%) and 3% head drop ($\Delta H$=3%) at three different flow rates. Cavitation is observed in the central region of the impeller, and as the Net Positive Suction Head (*NPSH*) decreases, it gradually expands toward the outer areas of the impeller. Under the same cavitation degree, higher flow rates result in increased void volumes and a more serious cavitation degree.

### 4.2 Time-Domain Feature Analysis Under Cavitation State

In this test, the vibration acceleration signals at five monitoring points were collected for three operating conditions. The rotational frequency of the pump during the test is about 48.3 Hz, i.e., one rotation period is about 0.02s. The root-mean-square value of the vibration acceleration signal, $Z_{rms}$, is used as the vibration intensity of the test pump under different operating conditions, with the following calculation formula:

$$Z_{rms} = \sqrt{\frac{1}{n}\sum_{i=1}^{n} x_i^2} \tag{7}$$

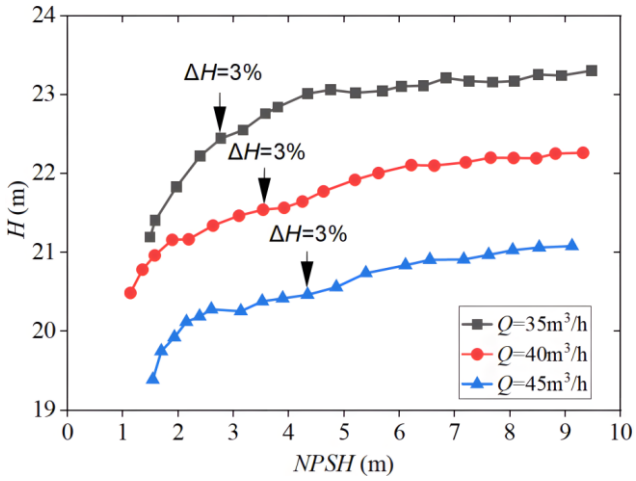


**Fig. 5 Head-drop curves with different flow rates**

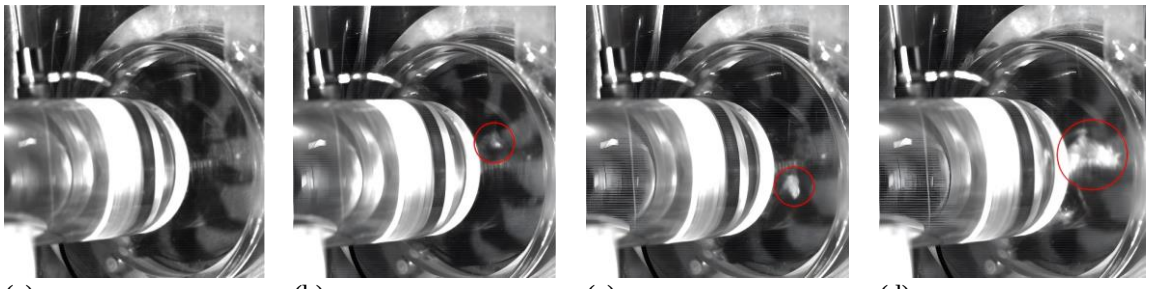

(a) (b) (c) (d)

**Fig. 6 Cavitation distribution of different *NPSH* at 35 $m^3/h$ flow rate: (a) non-cavitation (b) visual incipient cavitation (c) $\Delta H$=1% (d) $\Delta H$=3%**

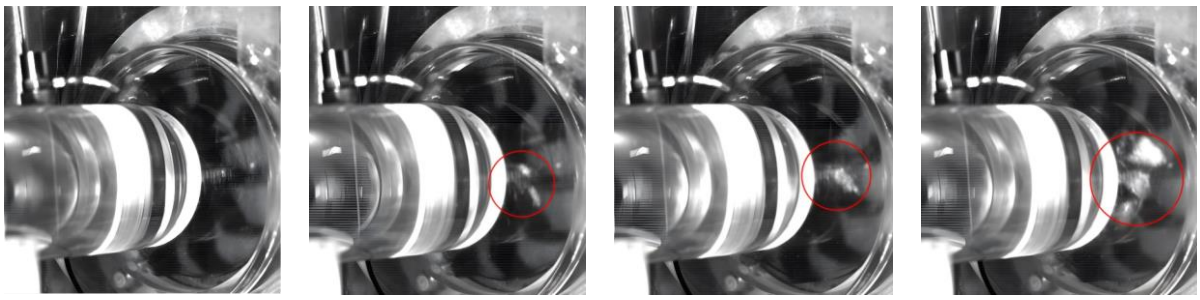

(a) (b) (c) (d)

**Fig. 7 Cavitation distribution of different *NPSH* at 40 m$^3$/h flow rate: (a) non-cavitation (b) visual incipient cavitation (c) Δ*H*=1% (d) Δ*H*=3%**

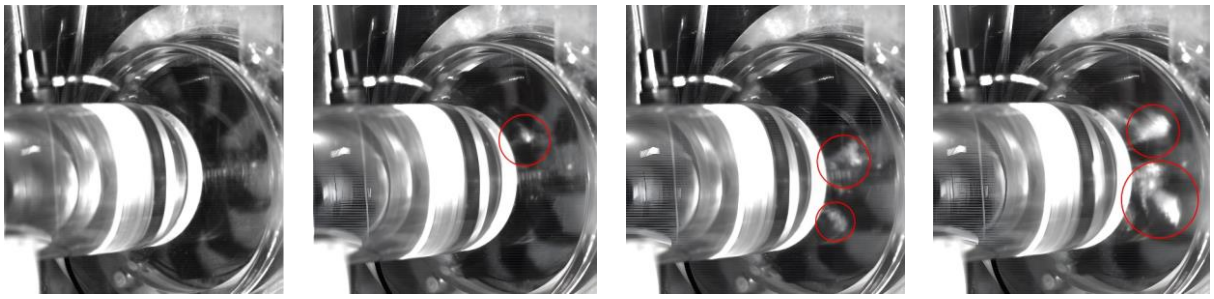

(a) (b) (c) (d)

**Fig. 8 Cavitation distribution of different *NPSH* at 45 m$^3$/h flow rate: (a) non-cavitation (b) visual incipient cavitation (c) Δ*H*=1% (d) Δ*H*=3%**

Where $x_i$ is the measured value of the vibration acceleration signal; $n$ is the number of sampling.

To obtain the vibration intensity change curve in the cavitation state of the vortex pump, the vibration acceleration signal collected in 1s is used as a calculation unit (i.e., 10,000 lengths of vibration acceleration signal), and the vibration intensity is calculated and plotted as a curve. Figure 9 illustrates the variation curve of vibration intensity with *NPSH* for the vortex pump under different operating conditions. As the *NPSH* decreases, the vibration intensity of the vortex pump increases in general and fluctuates up and down at the local operating condition. At the larger *NPSH*, the larger the flow, the greater the vibration intensity; at the smaller *NPSH*, the cavitation occurs in the vortex pump, and the cavitation bubble rupture generates vibration energy, resulting in intensified cavitation and more intense vibration. When operating under different *NPSH*, the vibrations are the most intense at the volute y-axis and z-axis; the maximum vibration intensity is 1.83 m/s$^2$ and 1.80 m/s$^2$, respectively. The vibration intensity is the second strongest at the outlet pipe z-axis and inlet pipe z-axis, and the vibration is the weakest at the volute x-axis. The vibration intensity increases with the flow rate increase at each monitoring point. The vibration intensity under the 45 m$^3$/h operating condition is consistently the largest throughout the cavitation experiment. At the lower *NPSH*, the vibration intensity under the 30 m$^3$/h operating condition is greater than that under the 40 m$^3$/h operating condition for all monitoring points except for the y-axis of the volute. The decrease in cavitation margin has the least impact on the rise in vibration intensity under the 40 m$^3$/h operating condition, particularly at the volute x-axis.

### 4.3 Frequency-domain feature analysis under cavitation state

The vortex pump's vibration is not a single simple harmonic vibration; rather, it is a periodic or quasi-periodic vibration that is modulated by several separate simple harmonic vibration frequencies. In the vortex pump, cavitation frequently causes vibration frequency characteristics to fluctuate. The FFT technique is widely employed for analyzing the spectrum of pump pressure pulsation or vibration (Zhou et al., 2019a,b; Zeng et al., 2022). Consequently, this research analyzes the cavitation-induced vibration signal in the frequency-domain. In this experiment, the vibration acceleration sensor is sampled at 10000 Hz, and the Nyquist sampling theorem allows for a maximum frequency range of up to 5000 Hz in the frequency-domain.

Figure 10 shows that the vibration amplitude is affected by the flow rate in the frequency range of 0-2000Hz, except for the outlet pipe's z-axis which shows significant rotational frequency. The flow rate affects the rotational frequency at the volute x-axis, y-axis, and z-axis. It has been observed that alterations in flow rate during cavitation can cause modifications to the frequency-domain features of the volute vibration signal. From the whole frequency range, the amplitude of each frequency band has different variations, and there are high-frequency segments within the frequency of 0-5000Hz. The high-frequency segments at the inlet pipe z-axis, volute y-axis, and volute z-axis are the most obvious, with frequencies ranging from 3000 Hz to 4500 Hz. This suggests that the vortex pump vibration caused by cavitation has a broad frequency characteristic, with different performance characteristics in different frequency ranges. Lu et al. (2017) suggested that this

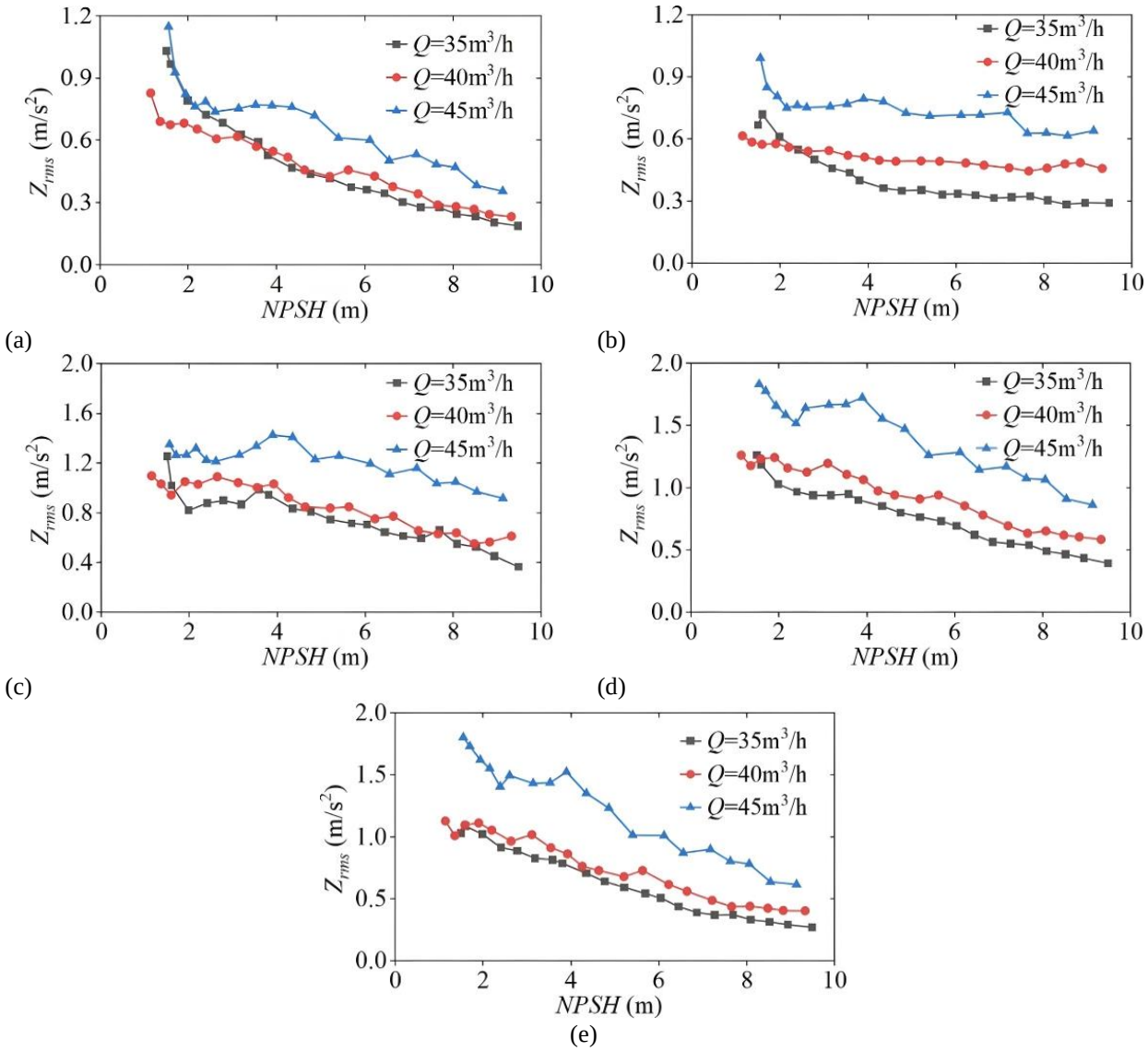


**Fig. 9 Vibration intensity distribution of vortex pump at different *NPSH:* (a) Outlet pipe z-axis (b) Volute x-axis (c) Inlet pipe z-axis (d) Volute z-axis (e) Volute y-axis**

broad frequency characteristic is caused by the unsteady motion of the fluid and the generation of surge and microjets between the rupture of the vacuole and the volute.

Figure 10 demonstrates that while the flow rate is between the 35 m$^3$/h and 40 m$^3$/h operating conditions, the dominant frequency is 580 Hz at the outlet pipe. Under the 45 m$^3$/h operating condition, the dominant frequency shifts to 350 Hz. The dominant frequency, which remains the rotational frequency, is constant at the x-axis of the volute. At the z-axis of the inlet pipe, the dominant frequency is 3900 Hz at all times. Under the 35 m$^3$/h operating condition, the dominant frequency is 1600 Hz at the volute z-axis, while under the 40 m$^3$/h and 45 m$^3$/h conditions, the dominant frequency is the rotational frequency. The dominant frequency is always twice that of the rotational frequency at the volute y-axis. It can be seen that the flow rate has little impact on the dominant frequency of cavitation-induced vibration at the volute x-axis and y-axis but increases the vibration amplitude at the dominant frequency. In short, the flow rate increases, making the cavitation more serious and causing more violent vibrations.

### 4.4 Time-Frequency Characteristics Analysis Under Cavitation State

The vibration acceleration signal produced by the vortex pump has non-stationary and non-linear properties. If only the frequency-domain and time-domain analyses are carried out, the local frequency-domain or time-domain characteristics of the signal might not be extracted, and the characteristics of the signal's frequency transformation with time cannot be effectively obtained. These characteristics will affect the identification of the cavitation state. The use of time-frequency analysis helps to study the characteristics of cavitation-induced vibration.

The STFT and AOK-TFR are contrasted on a portion of the vibration signal in the non-cavitation in this research, as illustrated in Fig. 11. The time-frequency graph generated by STFT displays low resolution and significant interference within the 0-5000 Hz frequency range. While the AOK-TFR does not have the window function restriction, the dominant frequency characteristics are obvious in the non-cavitation with good aggregation, making it easy to compare results with the

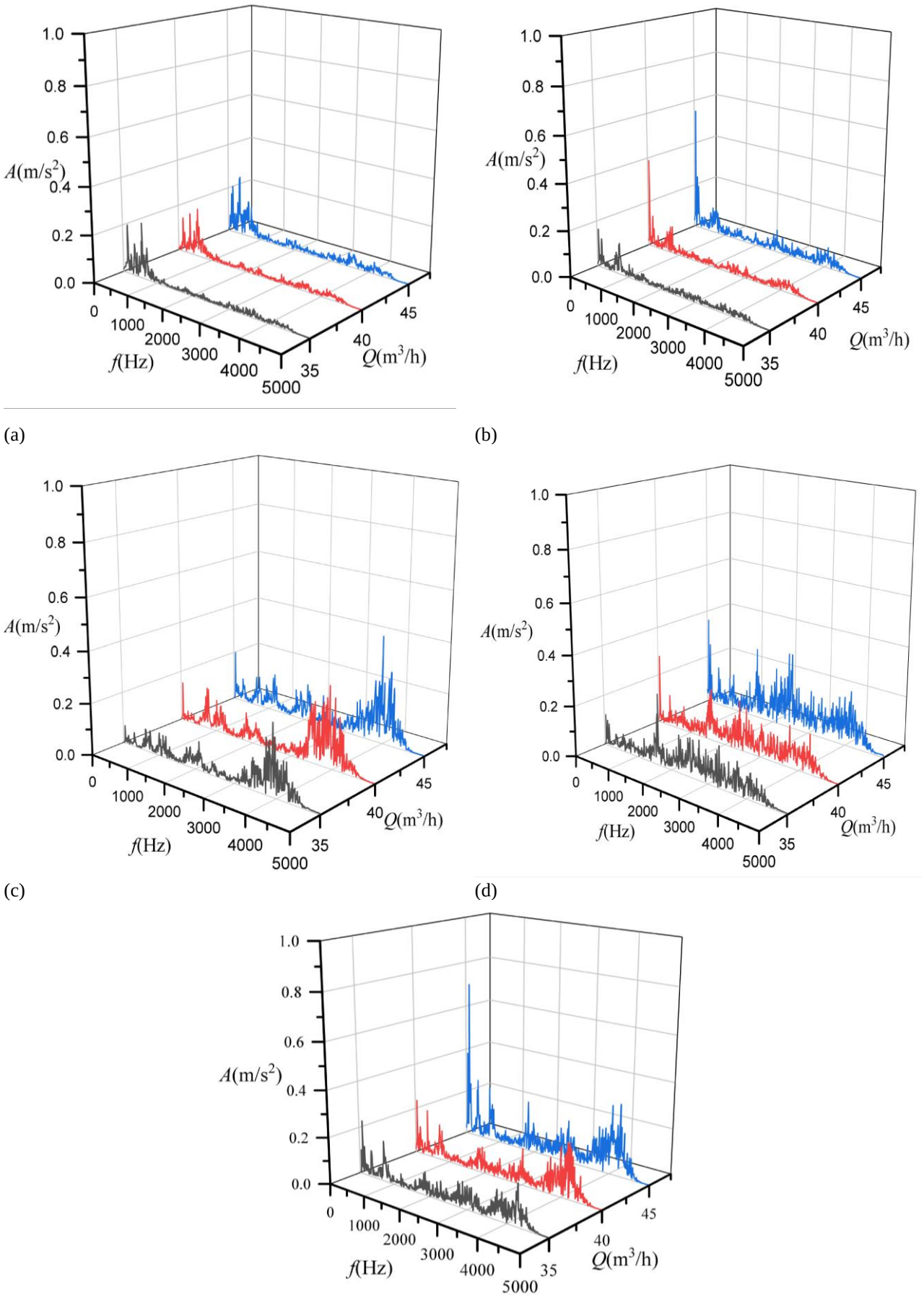


**Fig. 10. Frequency-domain diagram of test pump vibration signal at different flow rates under cavitation state: (a) Outlet pipe z-axis (b) Volute x-axis (c) Inlet pipe z-axis (d) Volute z-axis (e)Volute y-axis**

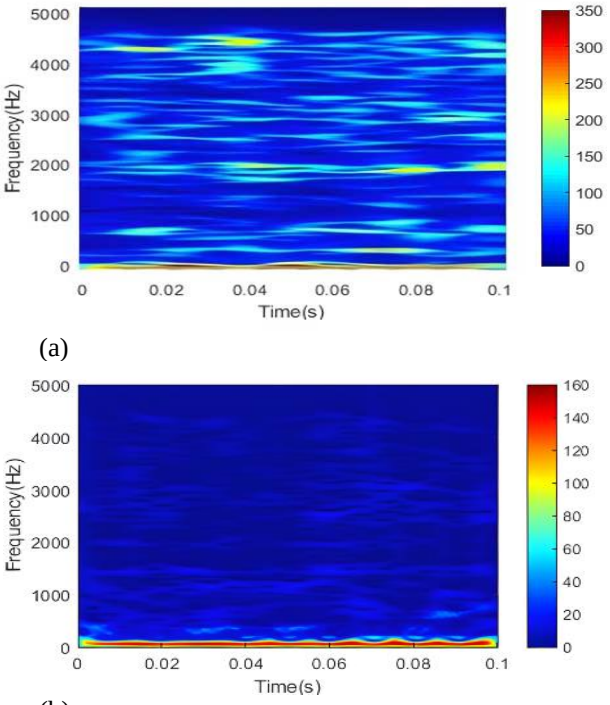


**Fig. 11 Comparison of different time-frequency analysis methods for vibration signals under non-cavitation state: (a) STFT (b) AOK TFR**

cavitated time-frequency distribution for analysis. The ideal time-frequency distribution should have good aggregation and be able to highlight the strong frequency changes.

The advantages of the AOK-TFR are threefold: (i) it has a high time-frequency resolution, which can more finely capture the transient process and frequency characteristic changes of the vortex pump's cavitation; (ii) it can capture detailed information about the cavitation vibration signal so that the evolution process of the cavitation phenomenon can be comprehensively analyzed; (iii) it can better distinguish the different frequency signals and restrain the mutual interference between multi-component signals. As a result, the AOK-TFR is useful for studying vortex pump cavitation development.

### 4.4.1 Analysis of Time-Frequency Characteristics Under Different Flow Rates

The characteristic signals of the inlet pipe z-axis and volute z-axis are not visible even at high flow rates. Therefore, the present work analyses the time-frequency domain of the z-axis of the outlet pipe, x-axis, and y-axis of the volute under various operating conditions. As Fig. 12 shows, the vibration frequency at the z-axis of the outlet is mainly concentrated in the range of 0-1000Hz, and the flow rate variation has little influence on the frequency band range. Under the 35 $m^3$/h operating condition, the dominant frequency is around 600 Hz ($1.2f_{BPF}$). Within 0.02s, there is a significant fluctuation in frequenc accompanied by a signal of 100 Hz ($2f_{RF}$), which is weaker and more chaotic in the domain. This is related to the unstable flow at the outlet caused by the volute asymmetry. Under the 40 $m^3$/h condition, the flow field inside the pump becomes quite stable. The dominant

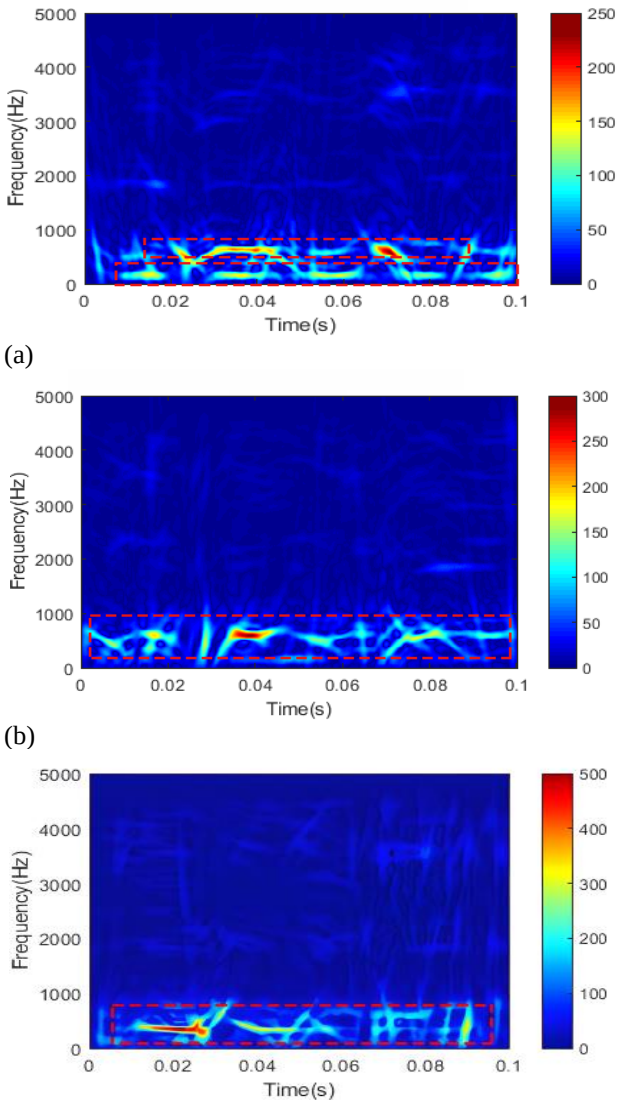


**Fig. 12. Time-frequency analysis of vibration acceleration signal in the z-axis of the outlet pipe when the head decreases by 3%: (a) $Q$=35 $m^3$/h (b) $Q$=40 $m^3$/h (c) $Q$=45 $m^3$/h**

frequency characteristics remain constant in the time-frequency diagram, while the $2f_{RF}$ signal gradually fades away. When the flow rate increased to 45 $m^3$/h, the dominant frequency decreased to 350 Hz ($7f_{RF}$) and the duration became longer.

Figure 13 shows that the rotational frequency signal in the x-axis of the volute has a good periodicity. The rotational frequency is the dominant frequency and is complemented by a frequency component of 700 Hz under the operating conditions of 35 $m^3$/h and 40 $m^3$/h. The rotational frequency component becomes more pronounced and lasts longer under the 45 $m^3$/h operating condition. In combination with Fig. 10 (b), it can be seen that the 700 Hz frequency band signal does not disappear, and its amplitude is relatively low compared with the dominant frequency. This is due to an increase in the dominant frequency amplitude as the flow rate increases.

As shown in Fig. 14, the frequency band at the y-axis of the volute is mainly concentrated in the range of 3800-

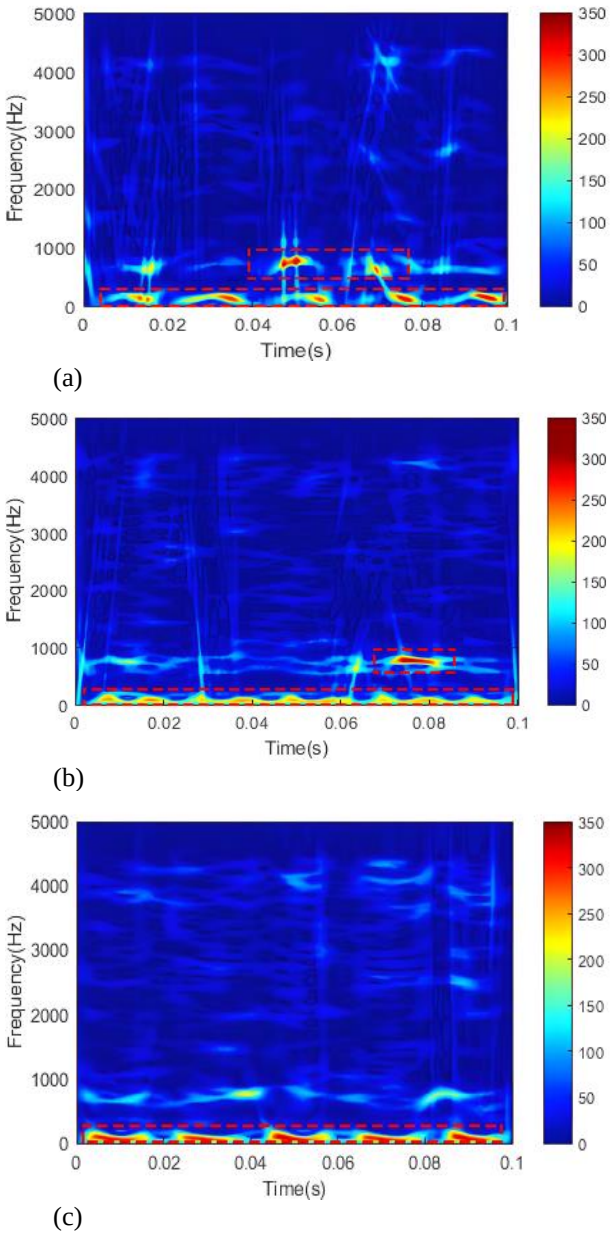


**Fig. 13. Time-frequency analysis of vibration acceleration signal of the volute x-axis when the head decreases by 3%: (a) $Q$=35 m$^3$/h (b) $Q$=40 m$^3$/h (c) $Q$=45 m$^3$/h**

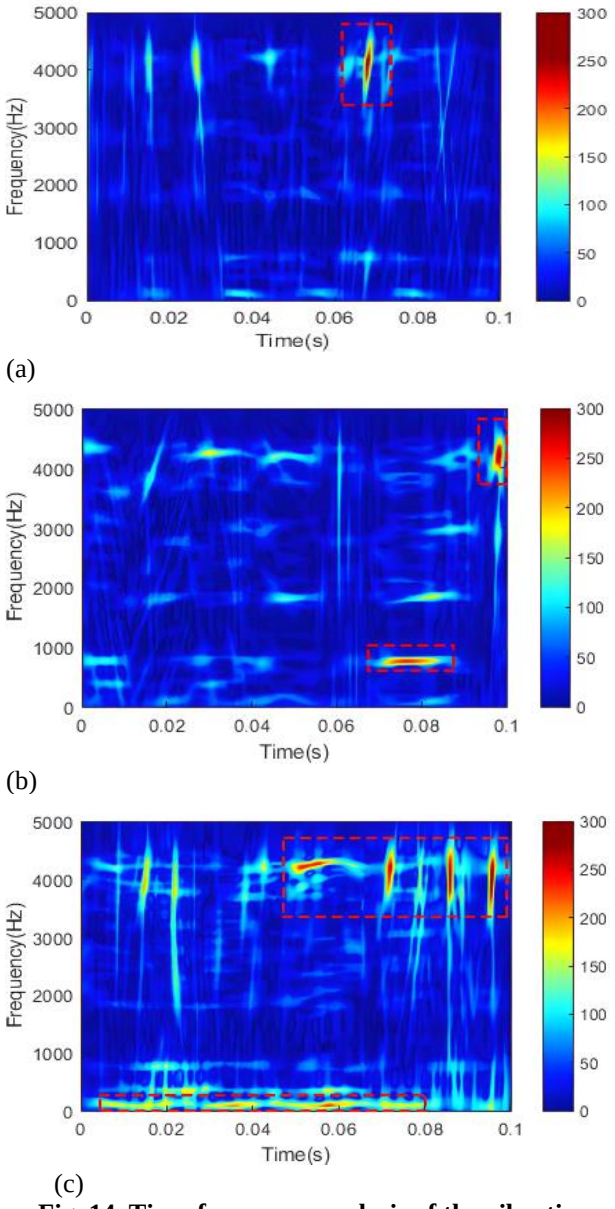


**Fig. 14. Time-frequency analysis of the vibration acceleration signal of the y-axis of the volute when the head decreases by 3%: (a) $Q$=35 m$^3$/h (b) $Q$=40 m$^3$/h (c) $Q$=45 m$^3$/h**

4300 Hz. It is possible that the volute rupture in the pump and the volute wall surface are causing vibration impacts. Under the 35 m$^3$/h operating condition, there is no obvious blade passing and rotational frequency. In the design operating condition, the frequency of 700 Hz appears and lasts longer in the time-frequency diagram. The rotational frequency is clearly enhanced under the 45 m$^3$/h condition, but the peak aggregation is weak.

### 4.4.2 Analysis of the Time-Frequency Characteristics Under Different Cavitation States

Figures 15-17 illustrate the results of using the vibration acceleration signals of various monitoring points for AOK-TFR to express the time-frequency diagram characteristics of vibration signals under different *NPSH*.

Figure 15 shows that the monitoring point exhibits evident fixed frequency band characteristics with significant aggregation and complicated modulation of the dominant frequency with time under various cavitation conditions in the frequency range of 200-1000Hz. Since the outlet pipe's z-axis is far from the volute, the rotational frequency is nearly undetectable on the time-frequency diagram. Under the visual incipient cavitation, the dominant frequency amplitude of the 200-1000Hz frequency band is enhanced. When the head decreases by 3%, this frequency band shows a complex aperiodic change and the frequency aggregation and duration are enhanced.

In Fig. 16, the rotational frequency signal is present in both non-cavitation and visual incipient cavitation and dominates the volute x-axis. Even when the head moves down by 1%, the rotational frequency remains dominant.

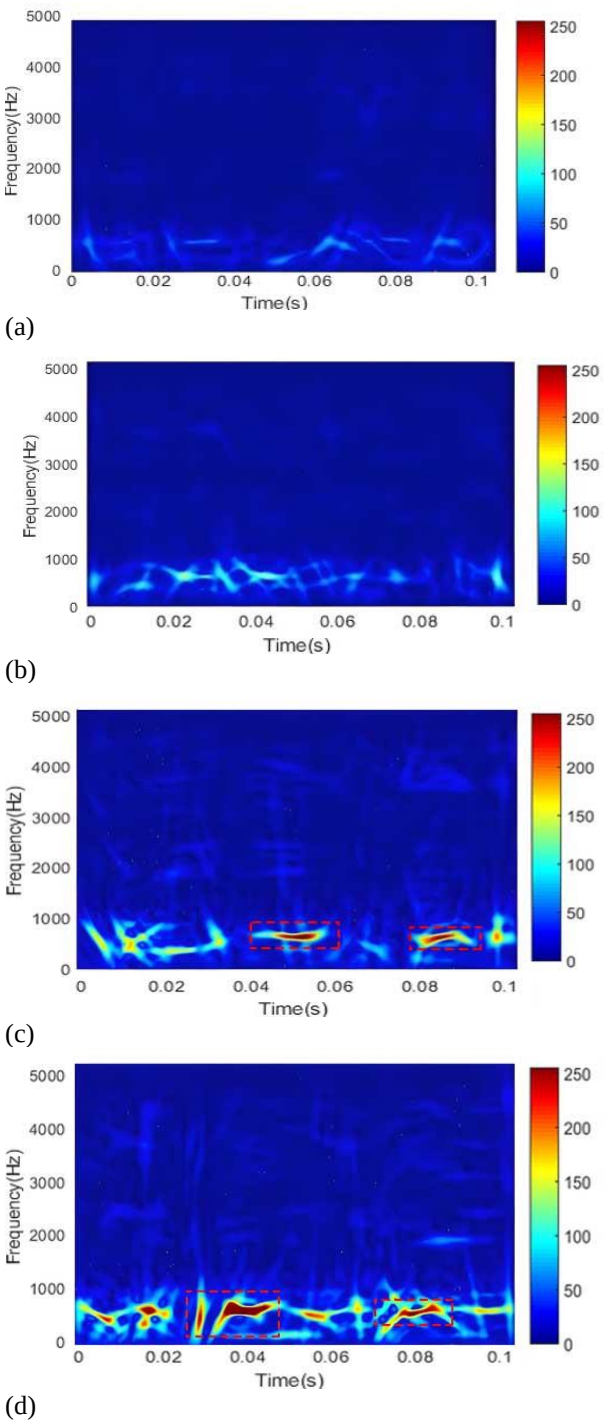


**Fig. 15. Time-frequency analysis of vibration acceleration signal of outlet pipe z-axis under operating condition: (a) non-cavitation (b) visual incipient cavitation (c) Δ*H*=1% (d) Δ*H*=3%**

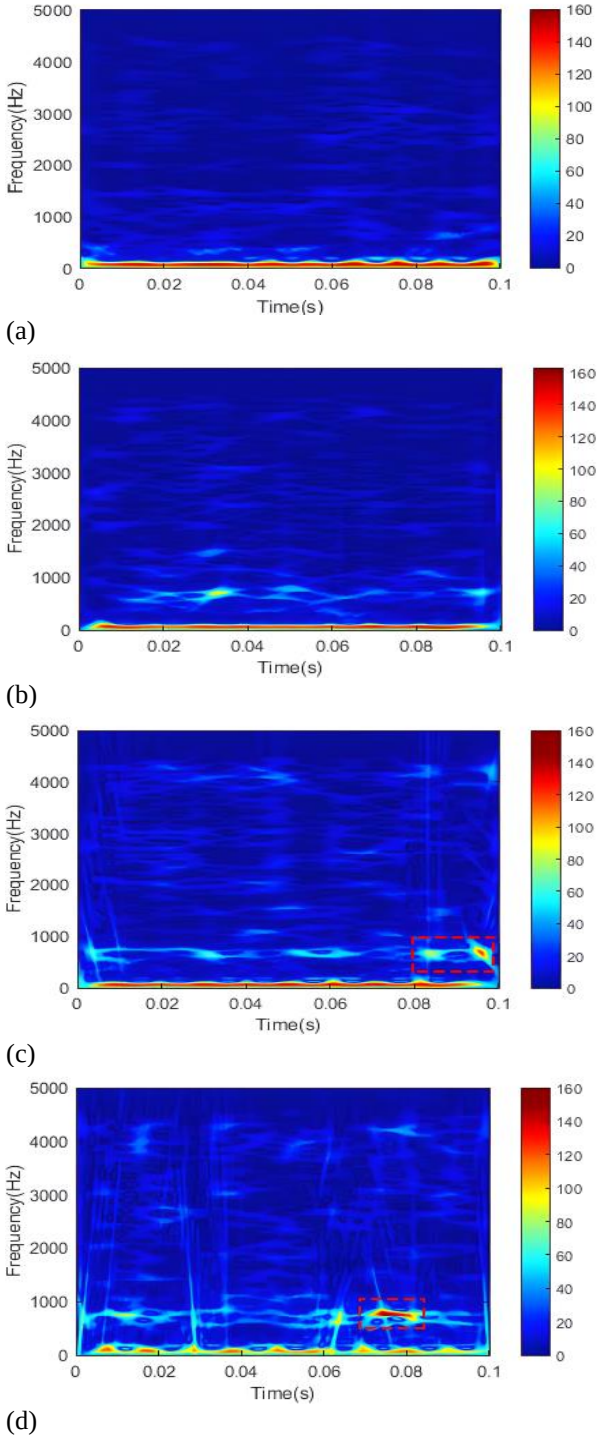


**Fig. 16. Time-frequency analysis of vibration acceleration signal of the volute x-axis under the operating condition: (a) non-cavitation (b) visual incipient cavitation (c) Δ*H*=1% (d) Δ*H*=3%**

However, a higher-amplitude frequency component with a shorter duration occurs at around 750 Hz (1.5 $f_{BPF}$), indicating the occurrence of cavitation. The special frequency signal may be attributed to the progressive development of the cavitation phenomenon, wherein the size of cavitation generated within the pump gradually increases and extends towards the blade outlet direction. Consequently, this leads to the eventual rupture of cavitation on the working surface of the blade and the subsequent generation of impact force. When the head drops below 3%, critical cavitation occurs, causing periodic fluctuations in the rotational frequency signal every 0.02s. The frequency aggregation at 750 Hz also increases substantially. In conclusion, the vibration signal of the volute x-axis is affected by the different cavitation states, causing distinct frequencies as cavitation intensifies.

As shown in Fig. 17, the dominant frequency at the y-axis of the volute is a rotational frequency that changes

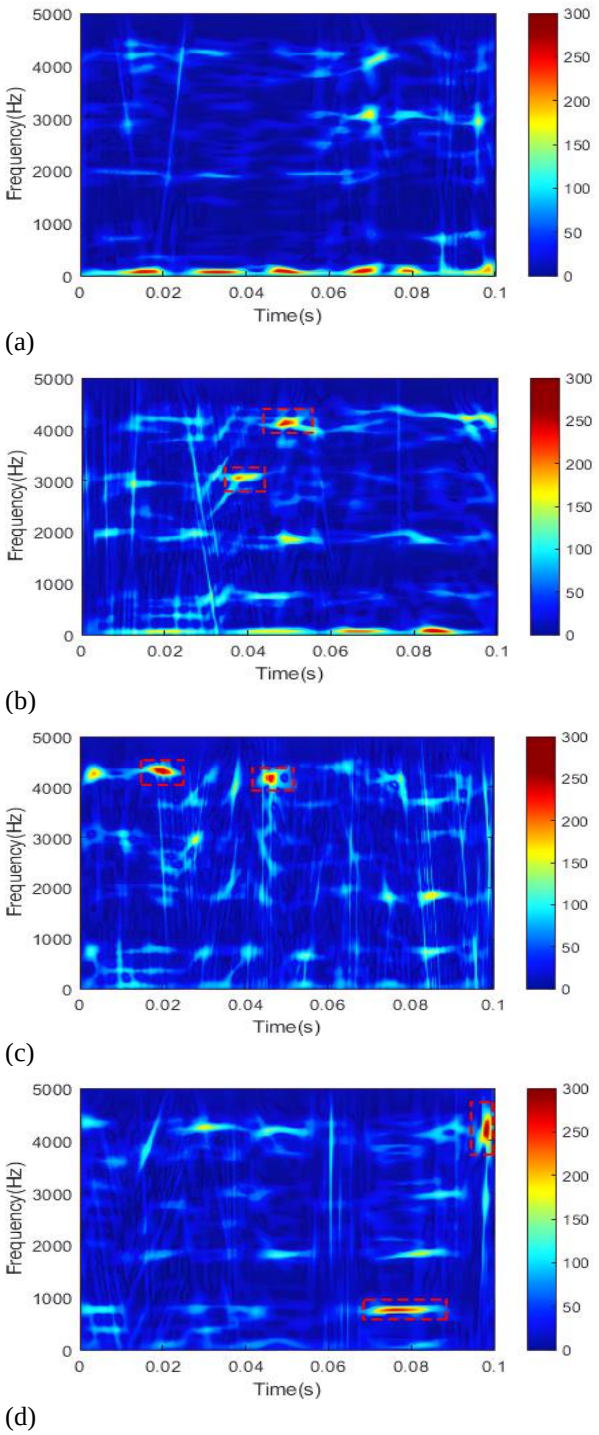


**Fig. 17. Time-frequency analysis of vibration acceleration signal of the volute y-axis under operating condition: (a) non-cavitation (b) visual incipient cavitation (c) Δ*H*=1% (d) Δ*H*=3%**

frequently with a weak high-frequency signal during non-cavitation. As cavitation increases, bubbles begin to form. The dominant frequency remains the rotational frequency. However, the time-frequency diagram shows a clear 4200 Hz and 3000 Hz frequency signal. It has been observed that at the y-axis of the volute, the degree of cavitation increases, resulting in the generation of broadband frequency because of the impact force produced by the bubble rupture. The peak is gathered at 4200 Hz when the head drops by 1% and the rotational frequency signal steadily declines. When the head drops down by 3%, the 750 Hz signal becomes observable while the rotational frequency becomes almost invisible in the time-frequency figure.

## 5. CONCLUSION

This study investigated the cavitation-induced vibration characteristics of a vortex pump through the collection and analysis of vibration signals at five monitoring points under three different flow rates. The main conclusions are as follows:

(1) The different flow rates significantly affect the cavitation-induced vibration signal of the vortex pump, with the vibration intensity under the 45 $m^3/h$ condition being higher than under the 35 $m^3/h$ and 40 $m^3/h$ conditions. As the *NPSH* decreases, the vibration energy resulting from the rupture of cavitation bubbles in the vortex pump increases, leading to a growth in vibration intensity. The volute y-axis and volute z-axis were identified as the locations with the most intense vibration, reaching maximum vibration intensity levels of 1.83 $m/s^2$ and 1.80 $m/s^2$, respectively.

(2) The amplitude of the frequency at each monitoring point showed a significant increase with the flow rate. Specifically, broad frequency characteristics were observed at the inlet pipe z-axis, volute y-axis and z-axis. These observations can be attributed to the presence of unsteady flow and the rupture of vacuoles.

(3) The AOK-TFR method exhibited better peak aggregation and highlighted stronger frequency variation, while also demonstrating a significant change in time-frequency characteristics with any change in flow rate. The rotational frequency was distinct at the volute x-axis and volute y-axis, and the frequency of 700 Hz (1.4 $f_{BPF}$) was found to be attenuated by the change in flow rate. As cavitation increased, frequency aggregation gradually intensified and a distinctive signal with a frequency of 750Hz (1.5 $f_{BPF}$) emerged in both the volute x-axis and the volute y-axis when the cavitation level dropped by 3% in the head. This may be due to the increased degree of cavitation leading to cavitation rupture and generating pressure.

## ACKNOWLEDGEMENTS

The authors gratefully acknowledge the financial support provided by the Welfare Technology Applied Research Project of Zhejiang Province (No. LGG21E090003), the Postdoctoral Science Foundation of Zhejiang Province (No. ZJ2021105), and China Postdoctoral Science Foundation (No. 2022M712816).

## CONFLICT OF INTEREST

The authors declare that they have no competing interests.

## AUTHORS CONTRIBUTION

**Yang Wang**: Writing-original draft and experimental research; **Peijian Zhou**: Conceptualization, project

administration and writing review; **Chengui Zhou**: Experimental research, formal analysis and resources; **Wenqiang Zhou**: Validation; **Jian Li**: Formal analysis.

## REFERENCES


Al-Obaidi, A. R. (2019). Investigation of effect of pump rotational speed on performance and detection of cavitation within a centrifugal pump using vibration analysis. *Heliyon*, *5*(6), e01910. https://doi.org/10.1016/j.heliyon.2019.e01910

Al-Obaidi, A. R. (2020). Detection of cavitation phenomenon within a centrifugal pump based on vibration analysis technique in both time and frequency domains. *Experimental Techniques*, *44*(3), 329-347. https://doi.org/10.1007/s40799-020-00362-z

Hajnayeb, A. (2021). Cavitation analysis in centrifugal pumps based on vibration bispectrum and transfer learning. *Shock and Vibration*, *2021*, 1-8. https://doi.org/10.1155/2021/6988949

Cao, R., Yuan, J., Deng, F., & Wang, L. (2021). Numerical method to predict vibration characteristics induced by cavitation in centrifugal pumps. *Measurement Science and Technology*, *32*(11), 115109. https://doi.org/10.1088/1361-6501/ac1181

Dai, C., Hu, S., Zhang, Y., Chen, Z., & Dong, L. (2023). Cavitation state identification of centrifugal pump based on CEEMD-DRSN. *Nuclear Engineering and Technology*, *55*(4), 1507-1517. https://doi.org/10.1016/j.net.2023.01.009

Jones, D. L., & Baraniuk, R. G. (1995). An adaptive optimal-kernel time-frequency representation. *IEEE Transactions on Signal Processing*, *43*(10), 2361-2371. https://doi.org/10.1109/78.469854

Li, N., Dong, S., Yang, D., & Hao, Z. (2009). *The research on frequency-hopping signals analysis methods based on adaptive optimal kernel time-frequency representation*. 2009 International Conference on Measuring Technology and Mechatronics Automation, IEEE. https://doi.org/10.1109/ICMTMA.2009.408

Li, W., G. (2017). A CFD predication of hydraulic and cavitation performance of a vortex pump as turbine. *Journal of Xihua University(Natural Science Edition)*, *36*(1), 60-68. https://doi.org/10.3969/j.issn.1673-159X.2017.01.012

Li, Y., Feng, G., Li, X., Si, Q., & Zhu, Z. (2018). An experimental study on the cavitation vibration characteristics of a centrifugal pump at normal flow rate. *Journal of Mechanical Science and Technology*, *32*, 4711-4720. https://doi.org/10.1007/s12206-018-0918-x

Lu, J., Yuan, S., Luo, Y., Yuan, J., Zhou, B., & Sun, H. (2016). Numerical and experimental investigation on the development of cavitation in a centrifugal pump. *Proceedings of the Institution of Mechanical Engineers, Part E: Journal of Process Mechanical Engineering*, *230*(3), 171-182. https://doi.org/10.1177/0954408914557877

Lu, J., Yuan, S., Parameswaran, S., Yuan, J., Ren, X., & Si, Q. (2017). Investigation on the vibration and flow instabilities induced by cavitation in a centrifugal pump. *Advances in Mechanical Engineering*, *9*(4), 1687814017696225. https://doi.org/10.1177/1687814017696225

Lu, Y., Tan, L., Han, Y., & Liu, M. (2022). Cavitation-vibration correlation of a mixed flow pump under steady state and fast start-up conditions by experiment. *Ocean Engineering*, *251*, 111158. https://doi.org/10.1016/j.oceaneng.2022.111158

Machalski, A., Skrzypacz, J., Szulc, P., & Błoński, D. (2021). *Experimental and numerical research on the influence of winglets arrangement on vortex pump performance*. Journal of Physics: Conference Series, IOP Publishing. https://doi.org/10.1088/1742-6596/1741/1/012019

Mao, W. Y., Song, P. Y., Deng, Q. G., & Xu, H. J. (2016). *Numerical simulation on the performance of the vortex pump for transporting solid-liquid two-phase with light particles*. IOP Conference Series: Materials Science and Engineering, IOP Publishing. https://doi.org/10.1088/1757-899X/129/1/012018

Sha, Y., & Hou, L., Y. (2010). Effect of impeller location and flow measurement in volute of a vortex pump. *Transactions of the Chinese Society for Agricultural Machinery*, *41*(11), 57-62. https://doi.org/10.3969/j.issn.1000-1298. 2010. 11. 011

Song, P. Y., Wang, H. L., & He, P. C. (2014). The numerical simulation and performance analysis of the vortex pump for solid-liquid two phase medium. *Applied Mechanics and Materials*, *527*, 88–92. https://doi.org/10.4028/www.scientific.net/amm.527.88

Steinmann, A., Wurm, H., & Otto, A. (2010). Numerical and experimental investigations of the unsteady cavitating flow in a vortex pump. *Journal of Hydrodynamics*, *22*(1), 319-324. https://doi.org/10.1016/S1001-6058(09)60213-4

Wu, X., F, Liu, Q, Sun, Y., L, Wang, Q & Gu, Y., Q. (2016). Experimental study on cavitation performance of the vortex pump. *General Machinery*, (4), 77-79. https://doi.org/10.3969/j.issn.1671 — 7139.2016.04.022

Yao, Z., Wang, F., Qu, L., Xiao, R., He, C., & Wang, M. (2011). Experimental investigation of time-frequency characteristics of pressure fluctuations in a double-suction centrifugal pump. *Journal of Fluids Engineering*, *133*(10), 101303. https://doi.org/10.1115/1.4004959

Zhou, R., Chen, H., Dong, L., Liu, H., Chen, Z., Zhang, Y., & Cheng, Z. (2022). Effect of vibration and noise measuring points distribution on the sensitivity of pump cavitation diagnosis. *Strojniški vestnik-Journal of Mechanical Engineering*, *68*(5), 325-338.

https://doi.org/10.5545/sv-jme.2022.59

Aoki, M. (1983). Studies on the Vortex Pump: 4th Report, Cavitation Characteristics. *Bulletin of JSME, 26*(216), 1020-1026. https://doi.org/10.1299/jsme1958.26.1020

Wang, Y., Zhou, P., Xu, N., Zhou, W., & Li, J. (2023). Recent advances in optimization design and performance analysis of vortex pumps. *Recent Patents on Mechanical Engineering*, *16*(3), 165-176. https://doi.org/10.2174/2212797616666230623111337

Zhou, P., Wu, Z., Mou, J., Wu, D., Zheng, S., & Gu, Y. (2019a). Effect of reflux hole on the transient flow characteristics of the self-priming sewage centrifugal pump. *Journal of Applied Fluid Mechanics*, *12*(3), 689-699. https://doi.org/10.29252/JAFM.12.03.29207

Zhou, P., Dai, J., Yan, C., Zheng, S., Ye, C., & Zhang, X. (2019b). Effect of stall cells on pressure fluctuations characteristics in a centrifugal pump. *Symmetry*, *11*(9), 1116. https://doi.org/10.3390/sym11091116

Zeng, Y., Yao, Z., Huang, B., Wu, Q., & Wang, F. (2022). Experimental investigation of the hydrodynamic damping of a vibrating hydrofoil in cavitating flow. *Ocean Engineering*, *266*, 112734. https://doi.org/10.1016/j.oceaneng.2022.112734